

# A Differential Theory of Radiative Transfer: Supplemental Document

CHENG ZHANG, University of California, Irvine  
 LIFAN WU, University of California, San Diego  
 CHANGXI ZHENG, Columbia University  
 IOANNIS GKIOULEKAS, Carnegie Mellon University  
 RAVI RAMAMOORTHY, University of California, San Diego  
 SHUANG ZHAO, University of California, Irvine

## 1 GENERALIZED DERIVATIONS

Recall that our derivations in §4 and §5 of the paper rely on the simplifying assumptions that (i) there is no zero-measure light source or perfectly specular surface; and (ii) the medium is non-emissive. We now discuss possible generalizations that relax some of these assumptions.

### 1.1 Point Light Sources

We now discuss how our derivations in §4 of the paper can be extended to support point sources. Other zero-measure light sources (e.g., directional) can be handled in a similar fashion.

For a uniform point source located at  $\mathbf{x}^{\text{light}}$  with intensity  $I^{\text{light}}$ , the in-scattered radiance  $L^{\text{ins}}$  becomes

$$L^{\text{ins}}(\mathbf{x}, \boldsymbol{\omega}) = \int_{\mathbb{S}^2} f_p(\mathbf{x}, -\boldsymbol{\omega}', \boldsymbol{\omega}) L^{(1)}(\mathbf{x}, \boldsymbol{\omega}') d\boldsymbol{\omega}' + \frac{V(\mathbf{x}, \mathbf{x}^{\text{light}}) T(\mathbf{x}, \mathbf{x}^{\text{light}}) f_p(\mathbf{x}, \mathbf{x} \rightarrow \mathbf{x}^{\text{light}}, \boldsymbol{\omega}) I^{\text{light}}}{\|\mathbf{x} - \mathbf{x}^{\text{light}}\|^2} \quad (1)$$

Recall that  $\mathcal{K}_T L^{\text{ins}}$  involves an integral of  $L^{\text{ins}}$  over a straight line. When  $L^{\text{ins}}$  takes the form of Eq. (1), it can have jump discontinuities along this line due to sudden changes in visibility  $V$ . In other words, when a straight line goes across hard volumetric shadow boundaries resulting from zero-measure light sources,  $L^{\text{ins}}$  will be discontinuous at the line-shadow intersections.

Given  $\mathbf{x} \in \Omega \setminus \partial\Omega$  and  $\boldsymbol{\omega} \in \mathbb{S}^2$ , let  $\Gamma(\mathbf{x}, \boldsymbol{\omega}) \subset (0, D)$  to contain all discontinuous locations of  $V(\mathbf{x} - \tau\boldsymbol{\omega}, \mathbf{x}^{\text{light}})$  with respect to  $\tau$  (for  $0 < \tau < D$ ). Then, according to Reynolds transport theorem (Theorem 1), the derivative of  $\mathcal{K}_T \mathcal{K}_C L$  becomes

$$\begin{aligned} & (\partial_\pi \mathcal{K}_T \mathcal{K}_C L)(\mathbf{x}, \boldsymbol{\omega}) \\ &= \int_0^D T(\mathbf{x}', \mathbf{x}) \left[ \sigma_s(\mathbf{x}') \dot{L}^{\text{ins}}(\mathbf{x}', \boldsymbol{\omega}) + \right. \\ & \quad \left. + ((\dot{\sigma}_s(\mathbf{x}') - \Sigma_t(\mathbf{x}, \boldsymbol{\omega}, \tau) \sigma_s(\mathbf{x}')) L^{\text{ins}}(\mathbf{x}', \boldsymbol{\omega})) \right] d\tau \quad (2) \\ & \quad + \dot{D} T(\mathbf{x}_0, \mathbf{x}) \sigma_s(\mathbf{x}_0) L^{\text{ins}}(\mathbf{x}_0, \boldsymbol{\omega}), \\ & \quad + \sum_{\tau \in \Gamma(\mathbf{x}, \boldsymbol{\omega})} \dot{\tau} T(\mathbf{x}', \mathbf{x}) \sigma_s(\mathbf{x}') \Delta L^{\text{ins}}(\mathbf{x}', \boldsymbol{\omega}), \end{aligned}$$

Authors' addresses: Cheng Zhang, University of California, Irvine, chengz20@uci.edu; Lifan Wu, University of California, San Diego, liw086@eng.ucsd.edu; Changxi Zheng, Columbia University, cxz@cs.columbia.edu; Ioannis Gkioulekas, Carnegie Mellon University, igkioule@andrew.cmu.edu; Ravi Ramamoorthy, University of California, San Diego, ravir@cs.ucsd.edu; Shuang Zhao, University of California, Irvine, shz@ics.uci.edu.

where  $\mathbf{x}' := \mathbf{x} - \tau\boldsymbol{\omega}$ , and

$$\Delta L^{\text{ins}}(\mathbf{x}', \boldsymbol{\omega}) = \lim_{\epsilon \rightarrow 0^-} L^{\text{ins}}(\mathbf{x}' - \epsilon\boldsymbol{\omega}, \boldsymbol{\omega}) - \lim_{\epsilon \rightarrow 0^+} L^{\text{ins}}(\mathbf{x}' - \epsilon\boldsymbol{\omega}, \boldsymbol{\omega}). \quad (3)$$

In general, similar to  $\dot{D}$ , the exact form of  $\dot{\tau}$  depends on  $\dot{\mathbf{x}}$  and the scene geometry.

### 1.2 Specular Surfaces

To handle specular surfaces, two extensions to our method depicted in the paper are needed.

First, due to specular reflection and refraction, discontinuities of radiance  $L(\mathbf{x}, \boldsymbol{\omega})$  with respect to  $\boldsymbol{\omega}$  (for fixed  $\mathbf{x}$ ) arises from not only geometric edges but also their virtual images. Thus, the edge integral terms (e.g.,  $B^{\text{ins}}$  in Eqs. (22) and (23) of the paper) need to also cover these “virtual edges” which could be difficult to detect.

Second, for non-specular surfaces, the reflected/refracted directions  $\boldsymbol{\omega}'$  are effectively variables of integrations (over  $\mathbb{S}^2$ ) and independent of the scene parameter  $\pi$  (i.e.,  $\dot{\boldsymbol{\omega}}' \equiv 0$ ). This has been discussed in the main paper. For specular surfaces, on the contrary,  $\boldsymbol{\omega}'$  is typically defined deterministically by the incident direction  $-\boldsymbol{\omega}$  (e.g.,  $\boldsymbol{\omega}'$  being the mirrored version of  $-\boldsymbol{\omega}$  for specular reflections). Thus, when  $\boldsymbol{\omega}$  or the mapping between  $\boldsymbol{\omega}$  and  $\boldsymbol{\omega}'$  is  $\pi$ -dependent, so will be  $\boldsymbol{\omega}'$ .

### 1.3 Volumetric Emission

For emissive media such as flame, the volumetric emission  $L^e$  in Eqs. (6) and (10) of the main paper becomes nonzero. In this case,  $\dot{L}^{(0)}$  derived in Eq. (30) of the paper needs to include an extra term  $\partial_\pi \mathcal{K}_T \sigma_a L^e$ , the scene derivative of transported volumetric emission. This term can be derived in a very similar fashion as Eq. (16) of the paper and equals

$$\begin{aligned} & \partial_\pi (\mathcal{K}_T \sigma_a L^e)(\mathbf{x}, \boldsymbol{\omega}) \\ &= \partial_\pi \int_0^D T(\mathbf{x}', \mathbf{x}) \sigma_a(\mathbf{x}') L^e(\mathbf{x}', \boldsymbol{\omega}) d\tau \\ &= \int_0^D T(\mathbf{x}', \mathbf{x}) \left[ \sigma_a(\mathbf{x}') \dot{L}^e(\mathbf{x}', \boldsymbol{\omega}) + \right. \\ & \quad \left. (\dot{\sigma}_a(\mathbf{x}') - \Sigma_t(\mathbf{x}, \boldsymbol{\omega}, \tau) \sigma_a(\mathbf{x}')) L^e(\mathbf{x}', \boldsymbol{\omega}) \right] d\tau \\ & \quad + \dot{D} T(\mathbf{x}_0, \mathbf{x}) \sigma_a(\mathbf{x}_0) L^e(\mathbf{x}_0, \boldsymbol{\omega}), \end{aligned} \quad (4)$$

where  $\Sigma_t$  follows the definition in Eq. (17) of the paper, and  $\dot{\sigma}_a$  takes the same form as Eq. (18):

$$\dot{\sigma}_a(\mathbf{x}') = \frac{\partial \sigma_a}{\partial \pi}(\mathbf{x}') + \langle \dot{\mathbf{x}}', \nabla \sigma_a(\mathbf{x}') \rangle, \quad (5)$$

with  $\nabla$  being the gradient operator.

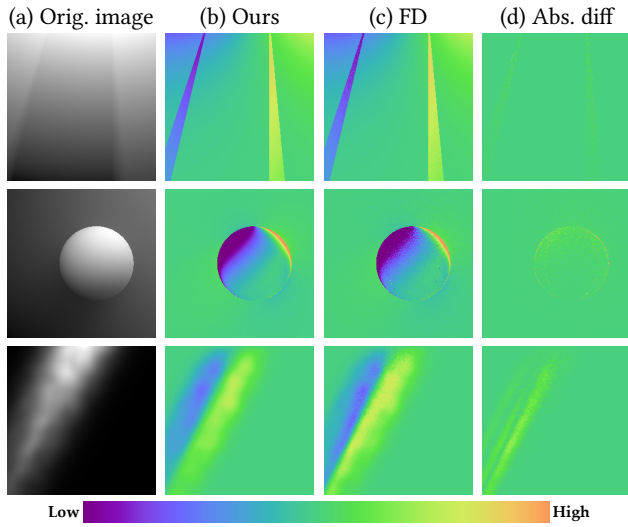


Fig. 1. **Comparisons** between derivative estimations generated by (b) our method and (c) finite difference (FD). The derivative values are encoded in false colors. Our results match the FD ones well with the discrepancies mostly due to FD’s bias.

## 2 PROOF-OF-CONCEPT RESULTS

We show proof-of-concept results for some of the generalized derivations from §1 as well as objects with higher-order surfaces (recall that our results in the main paper all use polygonal meshes). To this end, we configured three simple virtual scenes as follows.

*Point light source.* The first example contains a point light source and a triangular occluder. The virtual camera is configured to only look at the volumetric shadow casted by the occluder.

*Higher-order surface.* The second example involves a sphere embedded in an infinite homogeneous medium lit by an area source.

*Smooth dielectric interface.* The last example includes a smooth dielectric surface that encloses a heterogeneous medium and is lit by a collimated beam. The virtual camera focuses at the refracted beam within the medium.

### 2.1 Our Results

*Validation.* Figure 1 shows comparisons of derivatives estimated using our method and finite difference (FD). The derivatives visualized in this figure are taken with respect to (i) the displacement of the point source along the  $x$ -axis, (ii) the sphere center’s displacement along the  $x$ -axis, and (iii) the interface’s refractive index (IOR). Our results match the FD ones well with the differences mainly due to FD’s bias.

*Inverse rendering examples.* Figure 2 shows inverse rendering results using these examples. In the first example (i.e., point light source), we search for the 3D location of the light by only looking at the volumetric shadow casted by the occluder. In the second example, we optimize the 3D location of the sphere. In the last example, we optimize the refractive index (IOR) of the smooth dielectric interface.

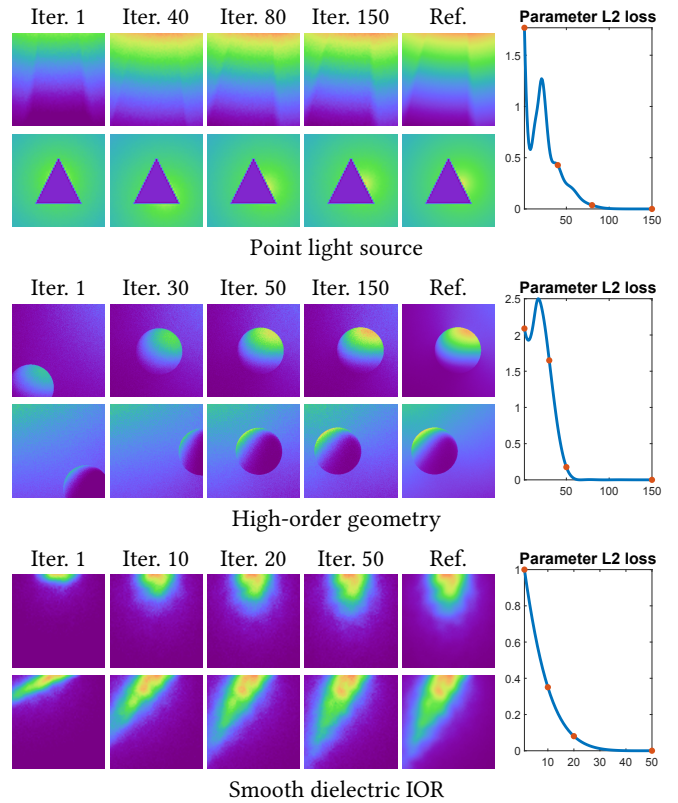


Fig. 2. **Inverse rendering results.** We search for scene parameters using gradients estimated with our technique. In each example, images on the top row are used for the optimizations. Those on the bottom row, on the contrary, are used to visualize the optimization process.

Optimizations driven by derivatives computed using our approach successfully recover the groundtruth parameters. Please refer to the supplemental material for animated versions of these results.